Supplementary Information.

Ultrasensitive Detection Enabled by Nonlinear Magnetization of Nanomagnetic Labels

M. P. Nikitin[1,2,3], A. V. Orlov[3], I. L. Sokolov[2], A. A. Minakov[3], P. I. Nikitin[3], J. Ding[1], S. D. Bader[1], E. A. Rozhkova[4], V. Novosad[1,5].

[1] Materials Science Division, Argonne National Laboratory, Argonne, IL 60439, USA.

[2] Moscow Institute of Physics and Technology, Dolgoprudny 141700, Russia.

[3] Prokhorov General Physics Institute, Moscow 119991, Russia.

[4] Center for Nanoscale Materials, Argonne National Laboratory, Argonne, IL 60439, USA.

[5] National University of Science and Technology (MISiS), Moscow, 119049, Russia.

Content:

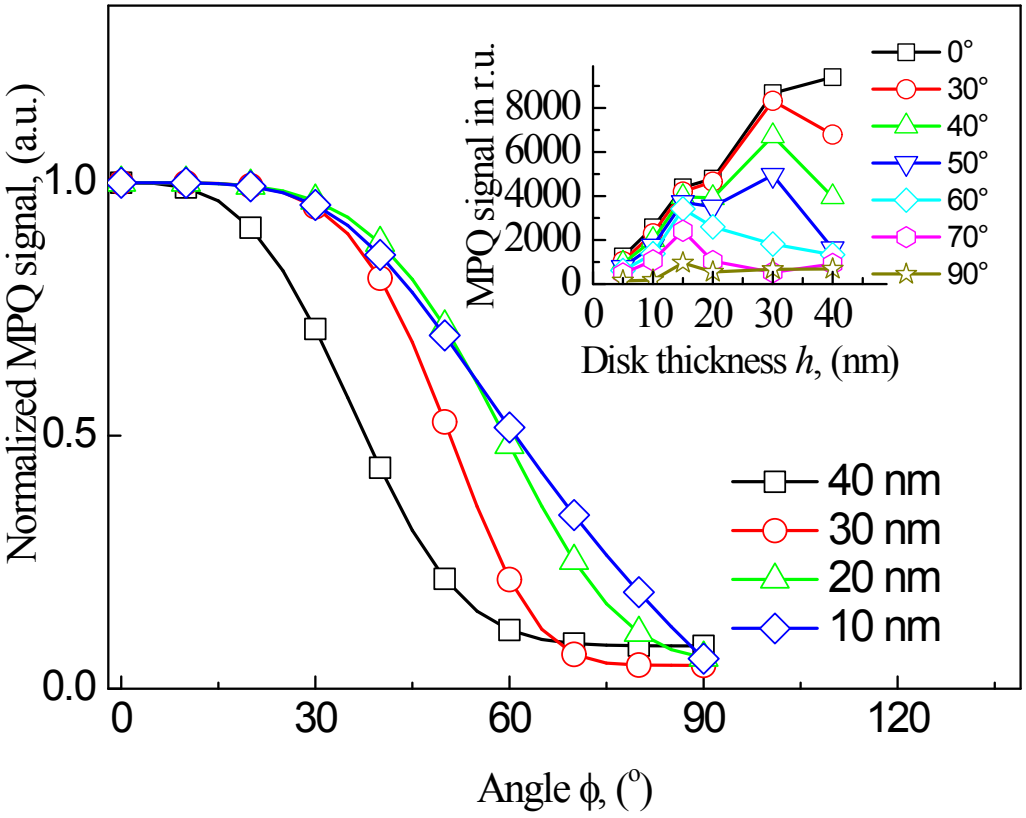

Fig. S1: Angular dependences of *normalized* MPQ sensor signal $S(h, \varphi)$ for the same parameters as in Fig. 4 at thicknesses h = 40 nm (squares), 30 nm (circles), 20 nm (up triangle), and 10nm (diamonds). The dependence of $S(h, \varphi)$ *vs*. h at $\varphi = 0°$ (squares), 30° (circles), 40° (up triangle), 50° (down triangle), 60° (diamonds), 70° (hexagons), 90° (stars) are shown in the insert.

III. **Analysis of hysteresis cycles in alternating magnetic fields**

The magnetization curves (see Fig. 2) can be described by descending $M_d(H_d)$ and ascending $M_a(H_a)$ branches of the hysteresis loops for descending H_d and H_a ascending magnetic fields. According to the Weierstrass approximation theorem, the descending and ascending branches can be approximated by polynomial functions:

$$M_d(H_d) = B_{0d} + B_{1d}H_d + B_{2d}H_d^2 + B_{3d}H_d^3 + B_{4d}H_d^4 + \dots , \quad \text{(s1)}$$

$$M_a(H_a) = B_{0a} + B_{1a}H_a + B_{2a}H_a^2 + B_{3a}H_a^3 + B_{4a}H_a^4 + \dots . \quad \text{(s2)}$$

A few major coefficients of Eq. (s1) and Eq. (s2) determined with a Mathcad program for normalized hysteresis loops are listed in Table S1.

Table S1 Primary coefficients of descending and ascending branches of the polynomial functions approximating the normalized hysteresis loop for nanodisks of 1.5 μm diameter and thickness *h*.

Thickness *h*, in nm	Branch	$10^5 \cdot B_1$, dimensionless	$10^5 \cdot B_2$, Dimensionless	$10^5 \cdot B_3$, dimensionless	$10^5 \cdot B_3 / B_1$, dimensionless
10	Descending	4499.4	91.15	0.7326	16.3
10	Ascending	4259.1	-146.0	2.2940	53.9
20	Descending	1463.8	24.73	1.1673	79.7
20	Ascending	1646.3	-33.24	0.8495	51.6
40	Descending	990.6	13.47	0.0839	8.5
40	Ascending	924.1	-12.38	0.1158	12.5

The result of the approximation of the hysteresis loops by the polynomial functions of thirteenth degree is shown in Fig. S2. The nonlinear terms of the 2nd and the 3rd degree in the descending and ascending branches of the hysteresis loops of the measured nanodisks are significant, which is essential for magnetic particle detection at combination frequencies of a double-component applied magnetic field. The signal at combination frequencies of the applied magnetic field arises due to the strong nonlinearity of the hysteresis loops of the circular magnetized nanodisks (see Fig. S32.

The polynomial functions $\mathsf{M}_d(H_d)$ and $\mathsf{M}_a(H_a)$ can be further utilized for estimation of the nonlinear response of the disks for a double-component alternating magnetic field:

$$H = H_1 \cdot \cos(2\pi f_1 \cdot t) + H_2 \cdot \cos(2\pi f_2 \cdot t), \qquad \text{(s3)}$$

where H_1, H_2, and f_1, f_2, are the amplitudes and the frequencies of the components of the applied magnetic field (the components are collinear), respectively. The model calculations were performed at frequencies f_1 = 150 Hz, f_2 = 150 kHz and amplitudes H_1 = 75 Oe, H_2 = 5 Oe for nanodisks of thickness h = 20 nm, as well as at H_1 = 150 Oe, H_2 = 10 Oe for h = 40 nm.

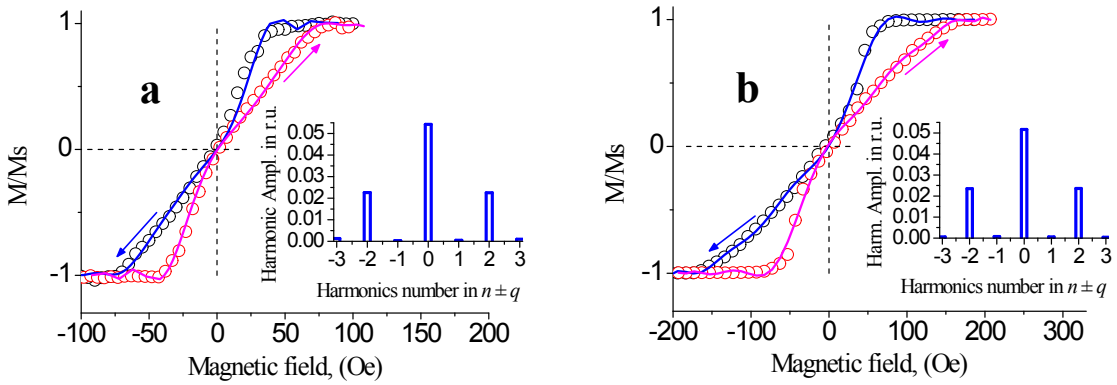

Fig. S2: The experimental hysteresis loops, the same as in Fig. 2 (circles), and polynomial functions (see Eq. (s1) and Eq. (s2)) approximating descending and ascending branches (solid lines) for the disk arrays of thickness h = 20 nm (**a**) and 40 nm (**b**). Amplitudes A_p of harmonic oscillations of the magnetic moment in the double-component alternating magnetic field at combination frequencies $f_p = (n \pm q) \cdot f_1$ for q = 0, 1, 2, 3 are shown in the inset.

The amplitudes A_p of harmonic oscillations of the magnetic moment $\mathsf{M}(H)$ at frequencies $p \cdot f_1$ in the double-component alternating magnetic field H can be calculated for the following function approximating the hysteresis loop:

$$\mathsf{M}(H) = \left\{\mathsf{M}_d(H) if \left\langle dH/dt \right\rangle_{AV} < 0\right\} \cup \left\{\mathsf{M}_a(H) if \left\langle dH/dt \right\rangle_{AV} > 0\right\}, \qquad \text{(s4)}$$

where $\langle dH/dt \rangle_{AV}$ is an average over the time interval $1/f_2$.

The amplitudes A_p averaged over the time interval $1/f_1$ (as measured in the experiment) were calculated as follows:

$$S_p = 2f_1 \int_0^{1/f_1} \mathsf{M}(H) \cdot \sin(2\pi p \cdot f_1 \cdot t) dt \,, \qquad \text{(s5)}$$

$$C_p = 2f_1 \int_0^{1/f_1} \mathsf{M}(H) \cdot \cos(2\pi p \cdot f_1 \cdot t) dt \,, \qquad \text{(s6)}$$

and $A_p = \sqrt{S_p{}^2 + C_p{}^2}$.

The model calculations were performed for $f_2 = n \cdot f_1$ at $n = 1000$. The harmonic amplitudes A_p at combination frequencies $f_p = (n \pm q) \cdot f_1$ for $q = 0, 1, 2, 3$ are shown in Fig. S2. Strong satellites of the driving harmonic $H_2 \cdot \cos(2\pi f_2 \cdot t)$ at frequencies $f_2 \pm 2l \cdot f_1$ (for $l = 1, 2, 3, \ldots$) arise due to the strong nonlinearity of the hysteresis-loop $\mathsf{M}(H)$. No satellites occur at frequencies $f_2 \pm (2l + 1) \cdot f_1$ because of odd symmetry of the complete cycle of the hysteresis-loop $\mathsf{M}(H)$. Fortunately, the detection and the filtering of the signal at frequencies $f_2 \pm 2l \cdot f_1$ are easier to perform when no satellites occur at frequencies $f_2 \pm (2l + 1) \cdot f_1$. Normally the signal at frequencies $f_2 \pm 2 \cdot f_1$ is detected in MPQ sensors.

Organs	**MPQ signal, (arb units)**	**Disks weight normalized to organ mass (ng/mg)**
Brain	16	0.062
Heart	24	0.028
Right kidney	0	0.000
Right thigh bone	9	0.004
Right thigh muscle	15	3.48
Skin	7	0.056
Spleen	533	29.8
Liver	808	131
Lungs	4865	60.5

Table S2: MPQ-based detection of the disks in the organs of mice *ex vivo* after retro-orbital administration of the disks.

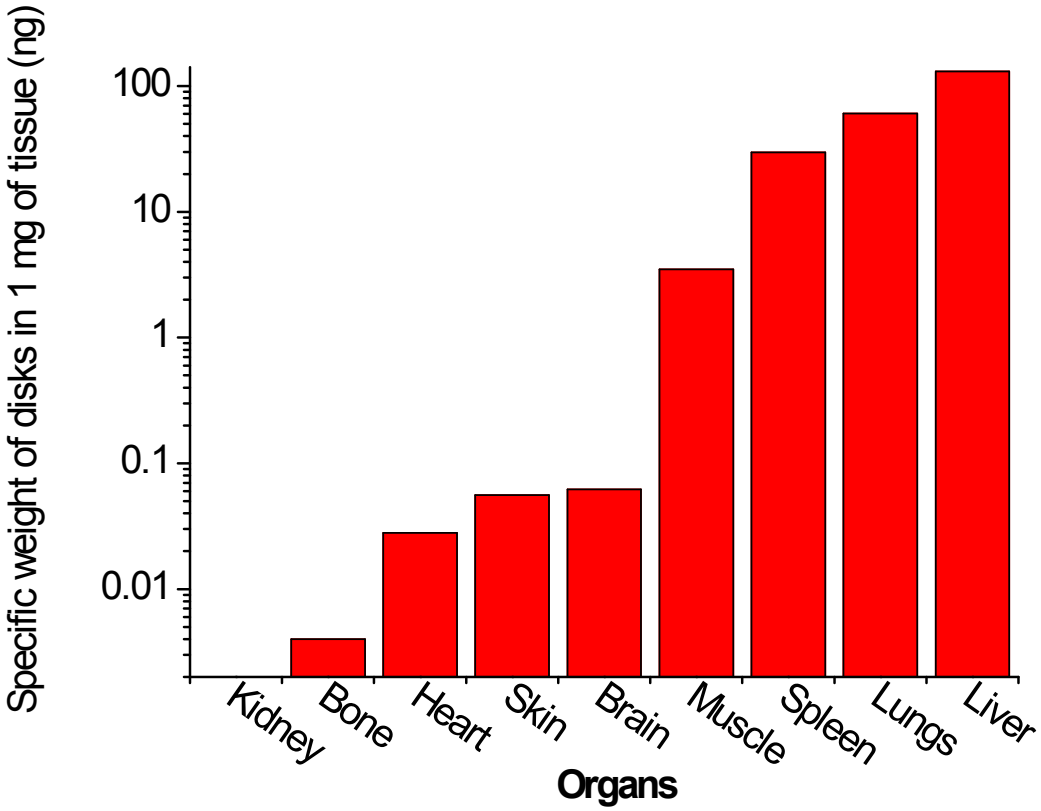

Figure S3 MPQ-based detection of the disks in the organs of mice *ex vivo* after retro-orbital administration of the disks (data taken from Table S1).

	Parallel	Before magnetization	Perpendicular 1	Perpendicular 1&2
Field scheme	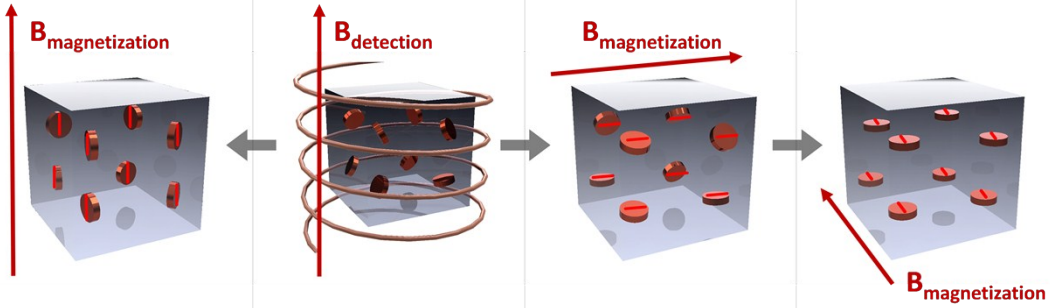			
Liver	1,59 ± 0,18	1	0,92 ± 0,02	0,88 ± 0,03
Spleen	1,35 ± 0,16	1	0,88 ± 0,07	0,77 ± 0,21
Lung	0,98 ± 0,03	1	0,98 ± 0,02	0,98 ± 0,01

Figure S4. MPQ-based detection of the rotation of the disks within the organs (liver, spleen, lungs) of mice injected with magnetic disks. The table shows changes in the MPQ-signals of the small pieces of each organ (n=3 pieces) after their magnetization with the field oriented parallel to the field of the MPQ detection coil (20-min magnetization), in one perpendicular direction (20-min magnetization) or subsequently in one perpendicular orientation (20-min) and then in the other perpendicular orientation (another 20 min). The scheme illustrates that magnetization in both perpendicular directions is needed to orient all disks perpendicular to the detection coil's field, and consequently is much harder to realize than magnetization in the parallel orientation.

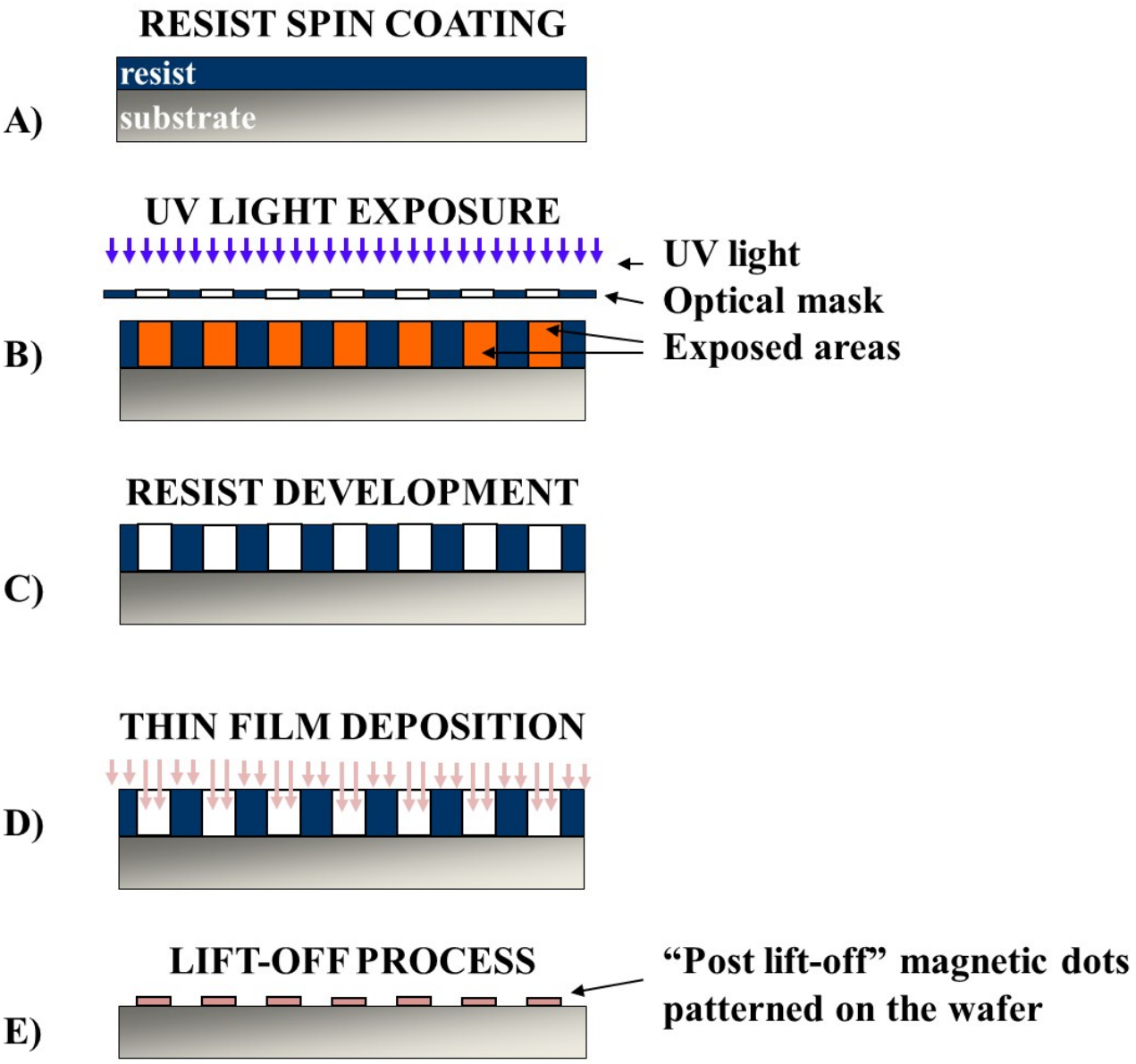

Figure S5. Scheme of samples preparation using optical lithography and magnetron sputtering. **A-E**. Patterned disks samples fabrication: the process starts with a positive tone photoresist spin coating on a silicon or GaAs wafer **(A)**. An optical mask is placed in contact with the layer of pre-baked photoresist and illuminated with UV light (**B**). An organic solvent dissolves and removes photoresist that is not exposed **(C)**. Magnetron sputtering is used to deposit a thin layer of magnetic material (**D**). After the lift-off process in an organic solvent, the patterned disk array is defined on the wafer (**E**). For biological experiments the negative tone resist is used instead, and, the disks are released from the wafer by a lift-off process.